

Integrating strong and weak discontinuities without integration subcells and example applications in an XFEM/GFEM framework

Sundararajan Natarajan^a, D Roy Mahapatra^b, Stéphane PA Bordas^{c,1},

^a*Cardiff School of Engineering Theoretical, Applied and Computational Mechanics, Cardiff University, Wales, U.K.*

^b*Assistant Professor, Department of Aerospace Engineering, Indian Institute of Science, Bangalore-560012, INDIA.*

^c*Professor, Cardiff School of Engineering Theoretical, Applied and Computational Mechanics, Cardiff University, Wales, U.K.*

Abstract

Partition of unity methods, such as the extended finite element method (XFEM) allow discontinuities to be simulated independently of the mesh [1]. This eliminates the need for the mesh to be aligned with the discontinuity or cumbersome re-meshing, as the discontinuity evolves. However, to compute the stiffness matrix of the elements intersected by the discontinuity, a subdivision of the elements into quadrature subcells aligned with the discontinuity is commonly adopted. In this paper, we use a simple integration technique, proposed for polygonal domains [2] to suppress the need for element subdivision. Numerical results presented for a few benchmark problems in the context of linear elastic fracture mechanics and a multi-material problem, show that the proposed method yields accurate results. Owing to its simplicity, the proposed integration technique can be easily integrated in any existing code.

Keywords: Schwarz Christoffel, conformal mapping, numerical integration, extended finite element method, quadrature, generalized finite element method, partition of unity finite element method, strong discontinuities, weak discontinuities, open-source MATLAB code.

¹Cardiff School of Engineering, Theoretical, Applied and Computational Mechanics, Cardiff University, Wales, U.K. Email: stephane.bordas@alumni.northwestern.edu. Tel. +44 (0)29 20875941.

1. INTRODUCTION

The classical finite element method (FEM) is one of the clear choices to solve problems in engineering and science. But the classical FEM approaches fail or are computationally expensive for some classes of problems, viz., equations with rough coefficients and discontinuities (arising e.g. in the reaction-diffusion equation, the advection-diffusion equation, crack growth problems, composites, materials with stiffeners etc.) and problems with highly oscillatory solutions viz., solution of Helmholtz's equation. In an effort to improve the FEM, Babuška *et al.*, [3] showed that the choice of non-polynomial ansatz functions, when tailored to the problem formulation, lead to optimal convergence, whereas the classical FEM, relying on the approximation properties of polynomials, performs poorly. Also in the case of Helmholtz's equation, Melenk [4] showed that plane waves displaying the same oscillatory behavior as the solution can serve as effective enrichment functions. This led to the birth of the Partition of Unity Method (PUM).

Belytschko's group in 1999 [1, 5], exploited the idea of partition of unity enrichment of finite elements (Babuška *et al.*, [3]) to solve linear elastic fracture mechanics problems with minimal remeshing. The resulting method, known as XFEM is classified as one of the partition of unity methods in which the main idea is to extend a classical approximate solution basis by a set of enrichment functions that carry information about the character of the solution (e.g., singularity, discontinuity, boundary layer).

As it permits arbitrary functions to be incorporated in the FEM or the mesh-free approximation, partition of unity enrichment [6, 7] leads to greater flexibility in modeling moving boundary problems, without changing the underlying mesh while the set of enrichment functions evolve (and/or their supports) with the interface geometry.

In PU type methods, the enrichment is extrinsic and resolved through additional degrees of freedom. The enrichment can also be intrinsic, based on the recent work by Fries and Belytschko [8]. In this paper, we focus on the extrinsic partition of unity enrichment and in general, the field variables are approximated by [1, 4, 9, 10, 6, 11, 7, 12]:

$$\mathbf{u}^h(\mathbf{x}) = \sum_{I \in \mathcal{N}^{\text{fem}}} N_I(\mathbf{x}) \mathbf{q}_I + \text{enrichment functions} \quad (1)$$

where $N_I(\mathbf{x})$ are standard finite element shape functions, \mathbf{q}_I are nodal variables associated with node I .

XFEM, one of the aforementioned partition of unity methods, was successfully applied for crack propagation and other fields in computational physics [13, 14, 15, 16, 17, 18, 19, 20, 21, 22] and recently open source XFEM codes were released to help the development of the method [23] and numerical implementation and efficiency aspects were studied [24]. XFEM is quite a robust and popular method which is now used for industrial problems [25] and under implementation by leading computational software companies. It is not the scope of this paper to review recent advances of partition of unity methods, and the interested readers are referred to the literature, for instance, Bordas and Legay [26], Karihaloo *et al.*, [27] and Belytschko *et al.*, [28].

Although XFEM is robust and applied to a wide variety of moving boundary problems, the flexibility provided by this class of methods also leads to associated difficulties:

- when the approximation is discontinuous or non-polynomial in an element, special care must be taken for numerical integration;
- the low order of continuity of the solution leads to poor accuracy (esp. in 3D) of the derivatives close to regions of high gradient, such as crack fronts [29] which motivated recent work on adaptivity for GFEM [30, 31], meshfree methods [32, 33, 34] and XFEM (Bordas and Duflot [35], Bordas *et al.* [36], Ródenas *et al.* [37]).

An important first attempt to simplify numerical integration was by Ventura [38], who focuses on the elimination of quadrature subcells commonly employed to integrate strongly or weakly discontinuous and non-polynomial functions present in the enriched FE approximation. His work is based on replacing non-polynomial functions by ‘equivalent’ polynomials. The proposed method is exact for triangular and tetrahedral elements, but for quadrilateral elements, when the opposite sides are not parallel, additional approximation is introduced.

Another method that alleviates this difficulty is strain smoothing [39, 40]. The main idea is to combine the smoothed finite element method (SFEM) [41, 42] with the XFEM. The SFEM relies on strain smoothing, which was proposed by Chen *et al.*, [43] for meshless methods, where the strain is written as the divergence of a spatial average of the standard (compatible) strain field

– i.e., symmetric gradient of the displacement field. In strain smoothing, the surface integration is transformed into an equivalent boundary integration by use of the Green-Ostrogradsky theorem. The Smoothed XFEM was introduced in [39], but much remains to be understood regarding the convergence, stability and accuracy of this method.

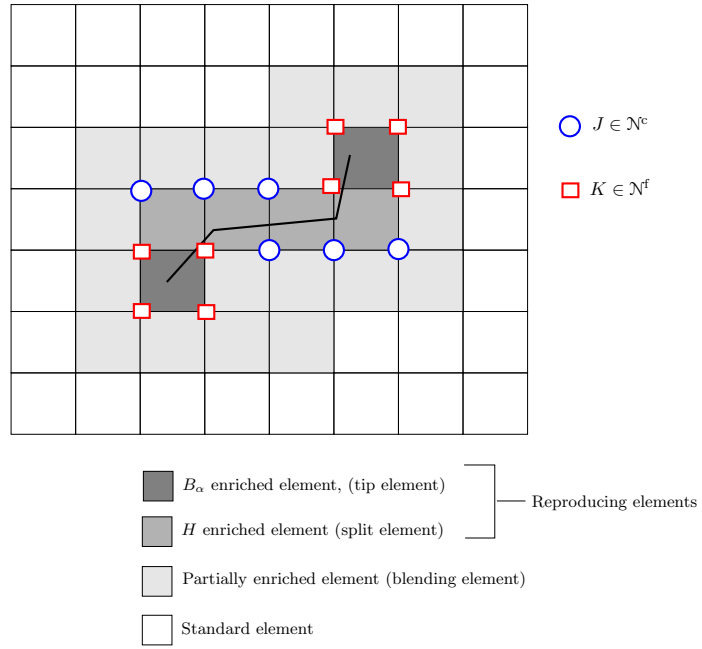
In this paper, we propose to use the new numerical integration technique proposed by the authors for arbitrary polygonal domains [2, 44, 45] to compute the stiffness matrix. Each part of the elements that are cut or intersected by a discontinuity is conformally mapped onto a unit disk using Schwarz-Christoffel mapping. A midpoint quadrature is used to obtain the integration points as opposed to the regular Gauß cubature rule. Thus, the proposed method which works only in 2D, eliminates the need to sub-divide the elements cut by discontinuities into quadrature subcells for the purpose of numerical integration of the stiffness matrix. The Schwarz-Christoffel mapping has been applied to mesh free Galerkin method by Balachandran *et al.*, [46] to obtain the weight function of the arbitrary shaped support domain obtained from natural neighbor algorithm.

The paper is organized as follows. In the next section, we briefly recall the basic equations of the XFEM. Section 3 will explain the new numerical integration scheme. The efficiency and convergence properties of the proposed method are illustrated in section 4 with a few benchmark problems taken from linear elastic fracture mechanics and a multi-material problem, which is followed by some concluding remarks in the last section.

2. BASICS OF PARTITION OF UNITY METHODS FOR DISCONTINUITIES AND SINGULARITIES

In this section, we give a brief overview of partition of unity methods in FEM for problems with strong and weak discontinuities. We focus on the extended FEM [1, 26], but the method is identical for alternatives such as the GFEM [30, 31].

With a regular finite element method, the mesh has to conform to the discontinuities and a very fine mesh is required in regions with sharp gradients. When the discontinuity surface evolves, cumbersome remeshing is required. The XFEM alleviates these difficulties by allowing the discontinuities to be independent of the mesh. An XFEM model consists of a regular FE mesh, which is independent of the discontinuity geometry. Figure (1) illustrates a typical FE mesh with a crack.



The main idea is to extend the approximation basis by a set of enrichment functions, that are chosen based on the local behavior of the problem. For the case of linear elastic fracture mechanics, two sets of functions are used: a Heaviside jump function to capture the jump across the crack faces and asymptotic branch functions that span the two-dimensional asymptotic crack tip fields. The enriched approximation for fracture mechanics problems takes the form [1, 26, 47]:

$$\mathbf{u}^h(\mathbf{x}) = \sum_{I \in \mathcal{N}^{\text{fem}}} N_I(\mathbf{x}) \mathbf{q}_I + \sum_{J \in \mathcal{N}^c} N_J(\mathbf{x}) H(\mathbf{x}) \mathbf{a}_J + \sum_{K \in \mathcal{N}^f} N_K(\mathbf{x}) \sum_{\alpha=1}^4 B_\alpha(\mathbf{x}) \mathbf{b}_K^\alpha, \quad (2)$$

where \mathbf{a}_J and \mathbf{b}_K are nodal degrees of freedom corresponding to the Heaviside function H and the near-tip functions, $\{B_\alpha\}_{1 \leq \alpha \leq 4}$, given by:

$$\{B_\alpha\}(r, \theta)_{1 \leq \alpha \leq 4} = \sqrt{r} \left\{ \sin\left(\frac{\theta}{2}\right), \cos\left(\frac{\theta}{2}\right), \sin(\theta) \sin\left(\frac{\theta}{2}\right), \sin(\theta) \cos\left(\frac{\theta}{2}\right) \right\}. \quad (3)$$

Nodes in set \mathcal{N}^c are such that their support is split by the crack and nodes in set \mathcal{N}^f belong to the elements that contain a crack tip. These nodes are enriched with the Heaviside and near-tip (branch functions) fields, respectively. In the discretization of Equation (2), the displacement field is global, but the supports of the enriching functions are local because they are multiplied by the nodal shape functions.

This modification of the displacement approximation does not introduce a new form of the discretized finite element equilibrium equation, but leads to an enlarged problem to solve:

$$\begin{bmatrix} \mathbf{K}_{uu} & \mathbf{K}_{ua} & \mathbf{K}_{ub} \\ \mathbf{K}_{au} & \mathbf{K}_{aa} & \mathbf{K}_{ab} \\ \mathbf{K}_{bu} & \mathbf{K}_{ba} & \mathbf{K}_{bb} \end{bmatrix} \begin{Bmatrix} \mathbf{q} \\ \mathbf{a} \\ \mathbf{b} \end{Bmatrix} = \begin{Bmatrix} \mathbf{f}_q \\ \mathbf{f}_a \\ \mathbf{f}_b \end{Bmatrix} \quad (4)$$

where the element stiffness matrix is given by:

$$\begin{bmatrix} \mathbf{K}_{uu}^e & \mathbf{K}_{ua}^e & \mathbf{K}_{ub}^e \\ \mathbf{K}_{au}^e & \mathbf{K}_{aa}^e & \mathbf{K}_{ab}^e \\ \mathbf{K}_{bu}^e & \mathbf{K}_{ba}^e & \mathbf{K}_{bb}^e \end{bmatrix} = \int_{\Omega^e} \begin{bmatrix} \mathbf{B}_{std}^T \mathbf{D} \mathbf{B}_{std} & \mathbf{B}_{std}^T \mathbf{D} \mathbf{B}_{enr}^1 & \mathbf{B}_{std}^T \mathbf{D} \mathbf{B}_{enr}^2 \\ (\mathbf{B}_{enr}^1)^T \mathbf{D} \mathbf{B}_{std} & (\mathbf{B}_{enr}^1)^T \mathbf{D} \mathbf{B}_{enr}^1 & (\mathbf{B}_{std}^1)^T \mathbf{D} \mathbf{B}_{enr}^2 \\ (\mathbf{B}_{enr}^2)^T \mathbf{D} \mathbf{B}_{std} & (\mathbf{B}_{enr}^2)^T \mathbf{D} \mathbf{B}_{enr}^1 & (\mathbf{B}_{std}^2)^T \mathbf{D} \mathbf{B}_{enr}^2 \end{bmatrix} d\Omega_e \quad (5)$$

where \mathbf{B}_{std} is the standard strain-displacement matrix, \mathbf{B}_{enr}^1 and \mathbf{B}_{enr}^2 are the enriched parts of the strain-displacement matrix corresponding to the Heaviside and asymptotic functions, respectively. \mathbf{D} is the material matrix.

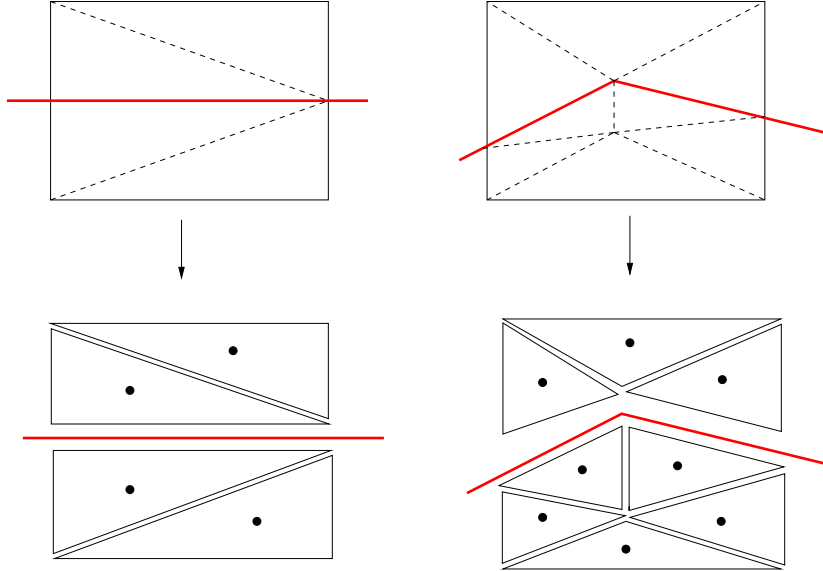


Figure 2: Integration in an element with a straight and kinked discontinuity: standard decomposition of an element for integration of a discontinuous weak form for XFEM. Gauß points are introduced within each triangle to ensure proper integration of the discontinuous displacement field.

The numerical integration of the stiffness matrix in elements intersected by a discontinuity, be it a material interface (weak discontinuity) or a crack (strong discontinuity) is not trivial. The standard Gauß quadrature cannot be applied in elements enriched by discontinuous terms, because the Gauß quadrature implicitly assumes a polynomial approximation. This is

circumvented by partitioning the elements into subcells aligned to the discontinuity surface, in which the integrands are continuous and differentiable (see Figure (2)). Although, the generation of quadrature subcells does not alter the approximation properties, it inherently introduces a ‘mesh’ requirement. The steps involved in this approach are: (1) Split the element into subcells with the subcells aligned to the discontinuity surface, usually the subcells are triangular (see Figure (2)) and (2) numerical integration is performed with the integration points from triangular quadrature. The subcells must be aligned to the crack or interface and this is costly and less accurate if the discontinuity is curved. Similar attempts were made to improve the integration of discontinuities in meshfree methods [48, 49, 50, 51, 52]. To alleviate this difficulty, we propose to use the new numerical integration technique proposed by the authors [2] for polygonal domains to integrate over the elements intersected by the discontinuity. The next section will briefly review the Schwarz-Christoffel conformal mapping (SCCM) and then discuss how to numerically integrate over elements intersected by discontinuities using the SCCM.

3. SCHWARZ-CHRISTOFFEL CONFORMAL MAPPING

Conformal mapping is extremely important in complex analysis and finds its application in many areas of physics and engineering. A conformal transformation or biholomorphic map is a transformation that preserves local angles. In other words, if Γ_1 and Γ_2 are two curves that intersect at an angle θ_z in the z -plane at a point p , then the images $f(\Gamma_1)$ and $f(\Gamma_2)$ intersect at an angle $\theta_w = \theta_z$ at $q = f(p)$. A Schwarz-Christoffel mapping is a transformation of the complex plane that maps the upper half-plane conformally to a polygon.

Definition 1. *A Schwarz-Christoffel map is a function f of the complex variable that conformally maps a canonical domain in the z -plane (a half-plane, unit disk, rectangle, infinite strip) to a ‘closed’ polygon in the w -plane.*

Consider a polygon in the complex plane. The Riemann mapping theorem implies that there exists a bijective holomorphic mapping f from the upper half plane $\{\zeta \in \mathbb{C} : \text{Im } \zeta > 0\}$ to the interior of the polygon. The function f maps the real axis to the edges of the polygon. If the polygon has interior angles $\alpha, \beta, \gamma, \dots$, then this mapping is given by,

$$f(\zeta) = \int^\zeta \frac{K}{(w-a)^{1-(\alpha/\pi)}(w-b)^{1-(\beta/\pi)}(w-c)^{1-(\gamma/\pi)} \dots} dw \quad (6)$$

where K is a constant, and $a < b < c < \dots$ are the values, along the real axis of the ζ plane, of points corresponding to the vertices of the polygon in the z plane. A transformation of this form is called a Schwarz-Christoffel mapping.

Recently, the authors proposed a new numerical integration technique [2, 44, 45] using the Schwarz-Christoffel mapping and cubature rules on a disk to numerically integrate over arbitrary polygons that arise in polygonal finite element methods. Figure (3) shows the conformal mapping of an arbitrary polygon onto a unit disk on which a midpoint rule [53] or Gauß Chebyshev rule [54] is used to obtain integration points. The distributions of integration points of the mid point quadrature and Gauß-Chebyshev quadrature are illustrated in Figure (4).

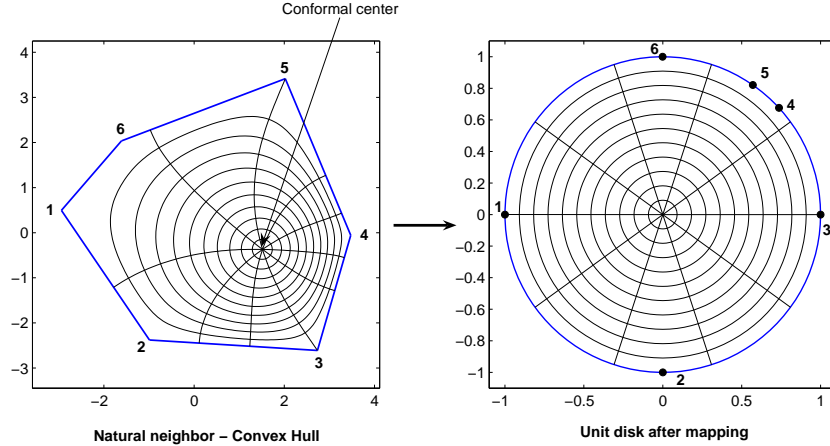
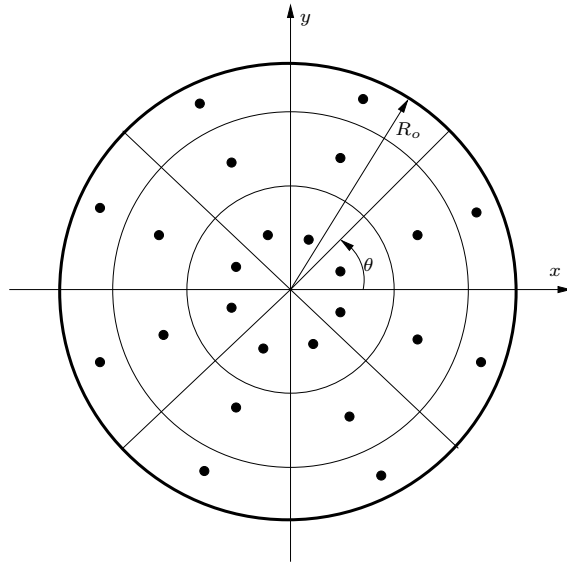
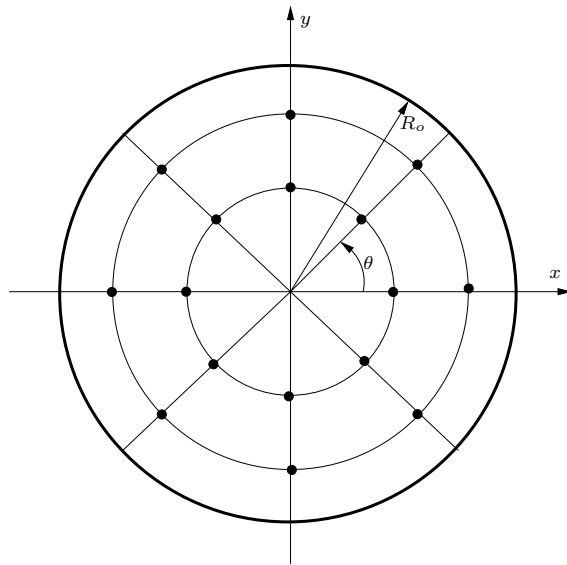


Figure 3: Mapping of the physical domain to the unit disk. This figure was produced with the MATLAB SC Toolbox [55]



(a) Midpoint rule



(b) Gauß-Chebyshev rule

Figure 4: Quadrature rules on a disk

In this paper, we propose to use conformal mapping in the context of the XFEM for 2D problems to numerically integrate over elements where the approximation or its derivatives is discontinuous. Each part of the element is conformally mapped onto a unit disk using the technique proposed in [2]. Figure (5) illustrates the above idea for split and tip elements.

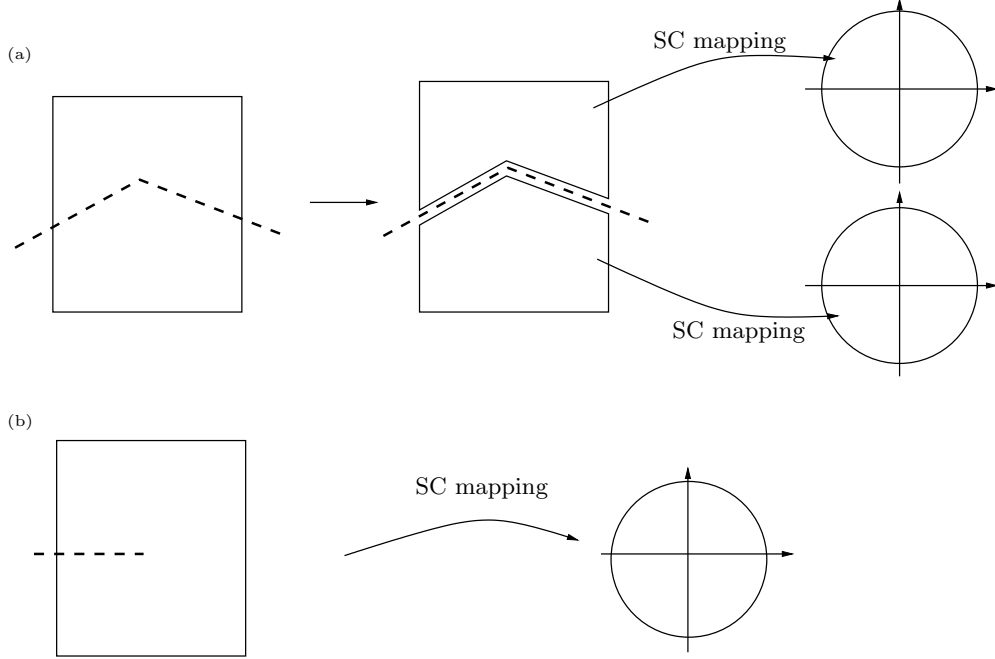


Figure 5: Integration over an element with discontinuity (dotted line): (a) with kinked discontinuity, representing the split element and (b) strong discontinuity, representing the tip element. In both cases, the sub-polygon is mapped conformally onto the unit disk using Schwarz-Christoffel conformal mapping.

One of the cubature rules mentioned above is used to obtain integration points. For elements that are not intersected by a discontinuity surface, the standard isoparametric mapping is implemented with four integration points for each element.

4. NUMERICAL EXAMPLES

In this section, we illustrate the effectiveness of the proposed method by solving a few benchmark problems taken from linear elastic fracture mechanics and a multi-material problem. We first consider an infinite plate under tension, then a plate with an edge crack, for which analytical solutions are available. Then, a multiple crack problem, followed by a multi-material problem is considered and as a last example crack growth in a double cantilever beam is studied. In this study, unless otherwise mentioned, quadrilateral elements² are used. In case of the XFEM with a standard integration approach, 13 integration points per subcell are used and a similar number of integration points are used for the SCCM, i.e., for a tip element with six subcells, 78 (=13 × 6) integration points are used for both methods. In this study, we use only topological enrichment, i.e., only the tip element is enriched by near tip functions [56, 57, 58].

4.1. Infinite plate under tension

Consider an infinite plate containing a straight crack of length a and loaded by a remote uniform stress field σ as shown in Figure (6). Along ABCD the closed form solution in terms of polar coordinates in a reference frame (r, θ) centered at the crack tip is

$$\sigma_x(r, \theta) = \frac{K_I}{\sqrt{r}} \cos \frac{\theta}{2} \left(1 - \sin \frac{\theta}{2} \sin \frac{3\theta}{2} \right) \quad (7a)$$

$$\sigma_y(r, \theta) = \frac{K_I}{\sqrt{r}} \cos \frac{\theta}{2} \left(1 + \sin \frac{\theta}{2} \sin \frac{3\theta}{2} \right) \quad (7b)$$

$$\sigma_{xy}(r, \theta) = \frac{K_I}{\sqrt{r}} \sin \frac{\theta}{2} \cos \frac{\theta}{2} \cos \frac{3\theta}{2} \quad (7c)$$

The closed form near-tip displacement field is:

$$u_x(r, \theta) = \frac{2(1+\nu)}{\sqrt{2\pi}} \frac{K_I}{E} \sqrt{r} \cos \frac{\theta}{2} \left(2 - 2\nu - \cos^2 \frac{\theta}{2} \right) \quad (8a)$$

$$u_y(r, \theta) = \frac{2(1+\nu)}{\sqrt{2\pi}} \frac{K_I}{E} \sqrt{r} \sin \frac{\theta}{2} \left(2 - 2\nu - \cos^2 \frac{\theta}{2} \right) \quad (8b)$$

²Bilinear element, 4 noded quadrilateral element

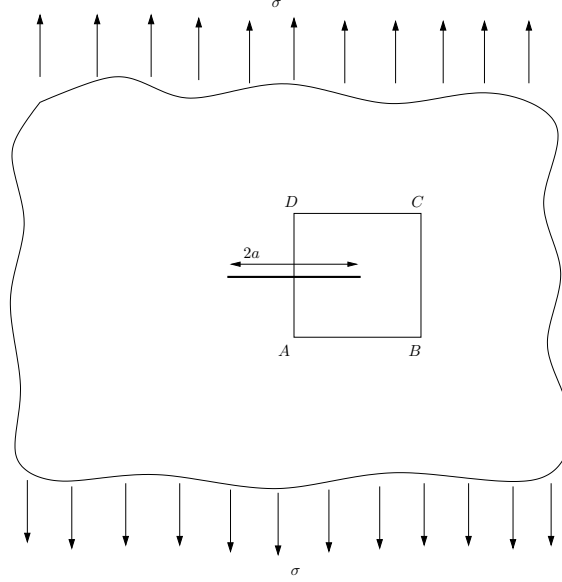


Figure 6: Infinite cracked plate under remote tension: geometry and loads

In the two previous expression $K_I = \sigma\sqrt{\pi a}$ denotes the stress intensity factor (SIF), ν is Poisson's ratio and E is Young's modulus. All simulations are performed with $a = 100\text{mm}$ and $\sigma = 10^4 \text{ N/mm}^2$ on a square mesh with sides of length 10mm .

Before carrying out the mesh convergence study and other numerical studies, the influence of the number of integration points in the tip element on the numerical SIF is studied. A structured quadrilateral mesh (60×60) is used for the study and the number of integration points are varied until the difference between two consecutive computations are less than a specified tolerance. During this study, the number of integration points for both methods are kept the same. The convergence of the SIF with the integration points is shown in Figure (7). It is seen that with the increase in the number of integration points, the SIF initially increases but reaches a constant value beyond 60 integration points.

The convergence and rate of convergence in numerical stress intensity factor are shown in Figure (8). It is seen that for the same number of integration points, the proposed method outperforms (although only slightly) the conventional XFEM. But with increase in mesh size, both techniques of

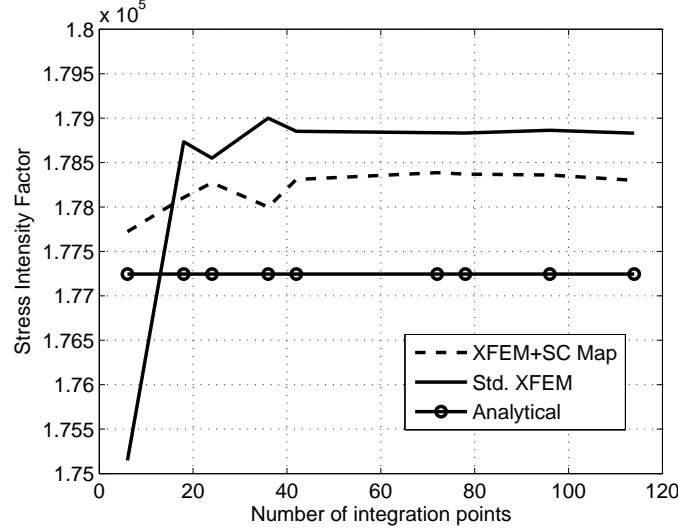


Figure 7: Griffith Problem: the convergence of the numerical stress intensity factor with number of integration points in the tip element. A structured quadrilateral mesh (60×60) is used.

numerical integration approach the analytical solution.

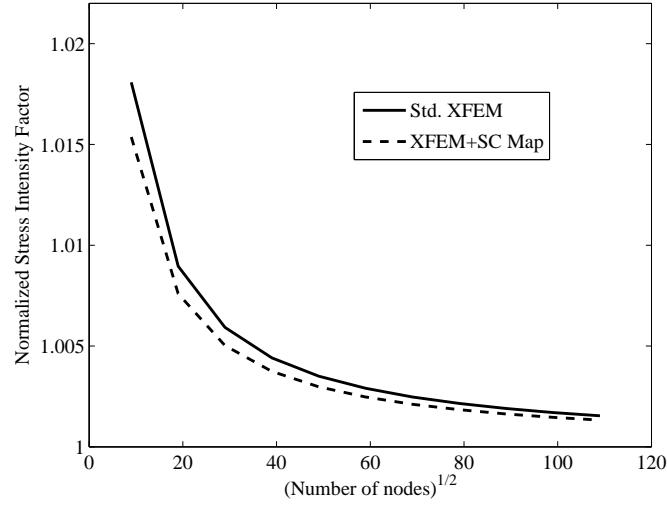
Examining Figure (8) shows that the convergence rates in the SIFs are suboptimal both for the XFEM with standard integration and the XFEM with the new integration technique proposed. This is for two reasons: (i) only the tip element is enriched (topological enrichment [29, 56, 57], which asymptotically reduces the XFEM approximation space to the standard FEM approximation space, this limits the optimal convergence rate to 0.5 in the presence of a square root singularity; (ii) no blending correction [59] is performed, which leads to yet a smaller convergence rate of 0.4, which is consistent with the literature [57, 60].

To demonstrate the effectiveness of the proposed method in case of skewed elements, the domain is meshed with irregular elements. The coordinates of interior nodes are given by

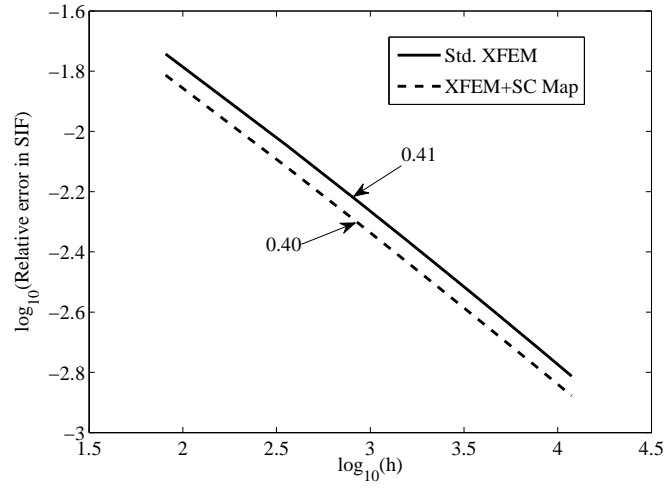
$$x' = x + (2r_c - 1)\alpha_{ir}\Delta x \quad (9a)$$

$$y' = y + (2r_c - 1)\alpha_{ir}\Delta y \quad (9b)$$

where r_c is a random number between 0 and 1.0, α_{ir} is an irregularity factor controlling the shapes of the distorted elements and $\Delta x, \Delta y$ are initial regular



(a)



(b)

Figure 8: Griffith Problem: the convergence of the numerical stress intensity factor to the analytical stress intensity factor and convergence rate.

element sizes in the x - and y -directions respectively. The discretization is shown in Figure (9).

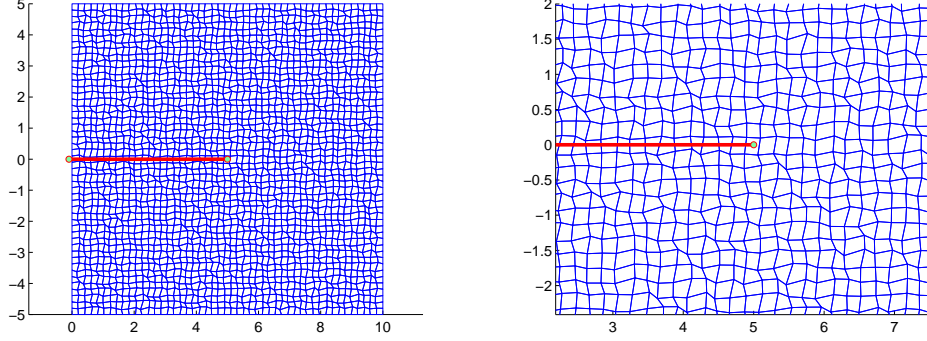


Figure 9: Polygonal mesh for infinite plate problem with a crack under uniform far field tension. The irregular mesh is generated with an irregularity factor, $\alpha_{ir} = 0.4$.

The convergence of the numerical stress intensity factor for the irregular mesh is shown in Figure (10). However, the convergence for distorted elements exhibits a non-uniform behavior. Results show that the results from both the numerical techniques are comparable. The advantage of the proposed method is that it eliminates the need to subdivide the split and the tip elements.

4.2. Edge crack under tension

A plate of dimension 1×2 is loaded by a tension $\sigma = 1$ over the top edge. The displacement along the y -axis is fixed at the bottom right corner and the plate is clamped at the bottom left corner. The geometry, loading, boundary conditions and domain discretization are shown in Figure 11. The reference mode I SIF is given by

$$K_I = F\left(\frac{a}{H}\right) \sigma \sqrt{\pi a} \quad (10)$$

where a is the crack length, H is the plate width and $F(\frac{a}{H})$ is an empirical function given as (For $(\frac{a}{H}) \leq 0.6$)

$$F\left(\frac{a}{H}\right) = 1.12 - 0.231\left(\frac{a}{H}\right) + 10.55\left(\frac{a}{H}\right)^2 - 21.72\left(\frac{a}{H}\right)^3 + 30.39\left(\frac{a}{H}\right)^4 \quad (11)$$

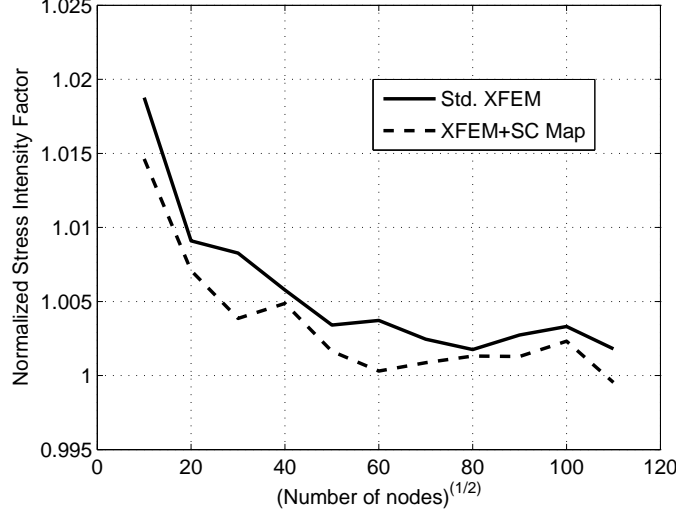


Figure 10: Griffith Problem: the convergence of the numerical stress intensity factor to the analytical stress intensity factor for distorted elements.

The convergence of the mode I SIF with mesh size and the rate of convergence of the SIF for a plate with an edge crack is shown in Figure (12). It is seen that with decrease in mesh density, both methods approach the analytical solution. Also, the proposed method performs slightly better than the standard XFEM. The rate of convergence for both methods is 0.4, very similar to the results available in the literature [1, 60, 56]. The rate of convergence can be improved by using a ‘geometrical’ enrichment as suggested by Béchet *et al.*, [56] or by modifying the enrichment functions such that they are zero in the standard elements and vary continuously in the blending elements as suggested by Fries [61].

In all the above examples, the background FE mesh is made up of regular quadrilateral elements. The numerical integration of the stiffness matrix over regular quadrilateral elements is not a difficult task. The real challenge is when the background mesh is made up of polygons or when the crack faces are irregular, i.e., when the crack faces cut the elements in such a way that at least one of the subdomains, created by the intersection of the geometry with the mesh, is a polygonal with more than 3 edges. To demonstrate the usefulness of the proposed integration technique, we consider the problem of inclined crack in tension with bilinear quadrilateral element as background FE mesh.

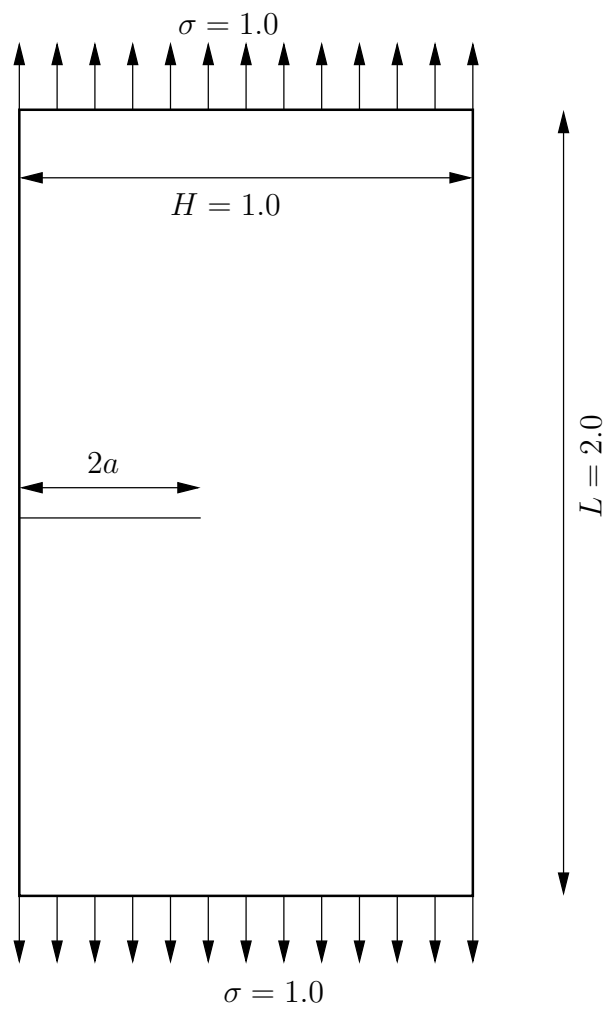
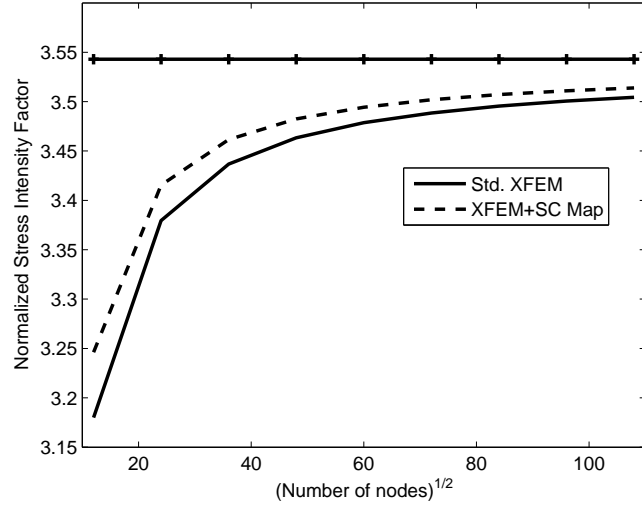
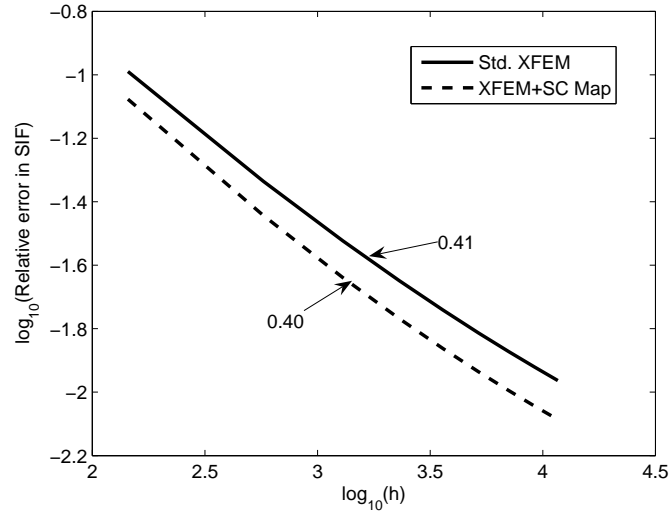


Figure 11: Plate with edge crack under tension



(a)



(b)

Figure 12: Edge crack problem: the convergence of the numerical stress intensity factor to the analytical stress intensity factor and convergence rate. Both the methods show a rate of convergence of 0.4, very close to the ones obtained in [56].

The study of problems involving polygonal FE meshes and arbitrary crack faces will be the topic of future papers.

4.3. Inclined crack in tension

Consider a plate with an angled crack subjected to a far field uniaxial stress field (see Figure (13)). In this example, K_I and K_{II} are obtained as a function of the crack angle β . For the loads shown, the analytical stress intensity factors are given by [62]

$$K_I = \sigma\sqrt{\pi a} \cos \beta \cos \beta, \quad K_{II} = \sigma\sqrt{\pi a} \cos \beta \sin \beta. \quad (12)$$

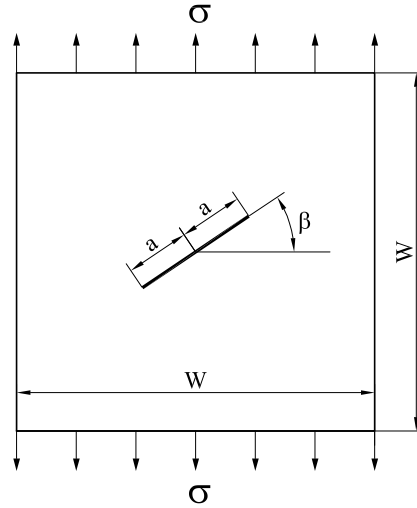


Figure 13: Inclined crack in tension

The influence of crack angle β on the SIFs is shown in Figure (14). A structured mesh (100×100) is used for the study. For crack angles, $0 < \beta < 90$, the crack face intersects the elements in such a way that one region of the split elements (either above or below the crack face) is a polygon. The polygonal subdomain is mapped onto a unit disk (see Figure (5)) instead of subdividing it into triangles. It is seen from Figure (14) that the numerical results are comparable with the analytical solution.

4.4. Multiple cracks in tension

In the next example, we consider a plate with two cracks. The geometry and boundary conditions of the problem are shown in Figure (15). In this

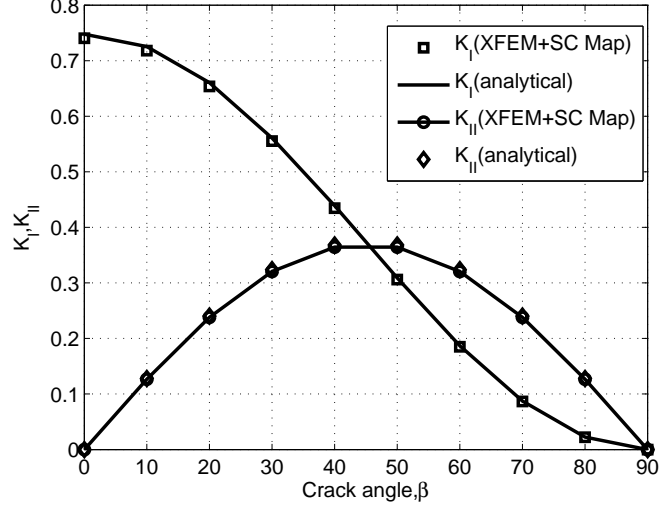


Figure 14: Variation of stress intensity factors K_I and K_{II} with crack angle, β .

case, the problem is solved only by the new proposed method. The material properties are: Young's modulus $E = 3 \times 10^7$ and Poisson's ratio, $\nu = 0.3$. A mesh size of 72×144 is used for the current study with crack size, $2a_1 = 0.2$. The length of the other crack $2a_2$ is varied.

Figure (16) shows the variation of the mode I SIF for different H/L ratios and for different ratio of crack lengths³ with $\theta_1 = 0$ and $\theta_2 = 0$, where θ_1 and θ_2 are the angles subtended by the crack faces with the horizontal (see Figure (15)). The normalized mode I SIF⁴ is plotted for point A in Figure (15). This is done to non-dimensionalize the results. Also, the value of $K_{\text{analytical}}$ is taken as the value for a plate with a center crack given by

$$K_I = \sigma \sqrt{\pi a \sec\left(\frac{\pi a}{2w}\right)} \quad (13)$$

where a is the half crack length, $w = \frac{W}{2}$ is the half width of the plate, and σ is the far field tensile load applied at the top of the plate.

It can be seen that with increase in the H/L ratio, the interaction between the cracks decreases, which is as expected. It is also seen from Figure

³crack length ratio = $\frac{2a_2}{2a_1}$

⁴ $K_{\text{normalized}} = \frac{K_{\text{numerical}}}{K_{\text{analytical}}}$

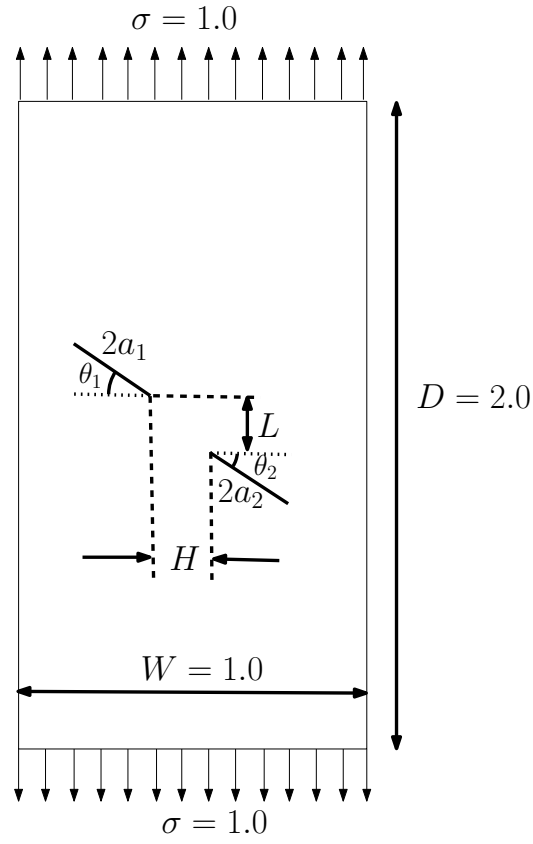


Figure 15: Plate with multiple cracks: geometry and loads. The length of the cracks are $2a_1$ and $2a_2$. θ_1 and θ_2 are the angles subtended by the crack faces with the horizontal.

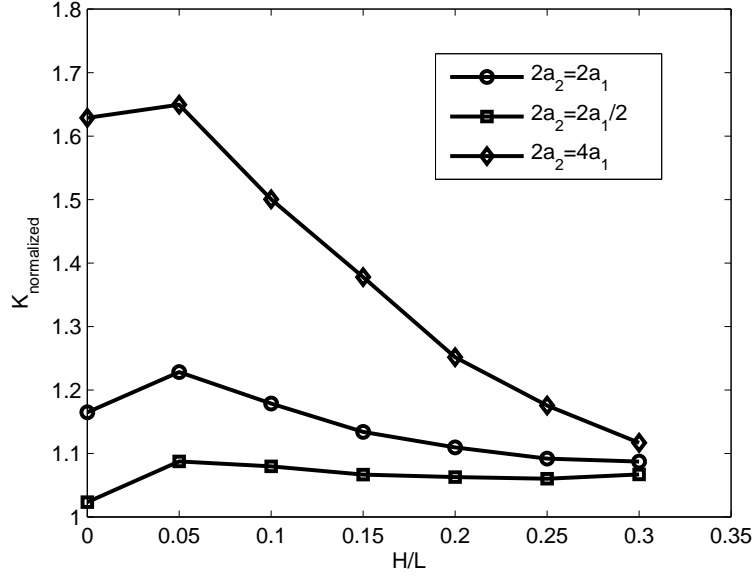


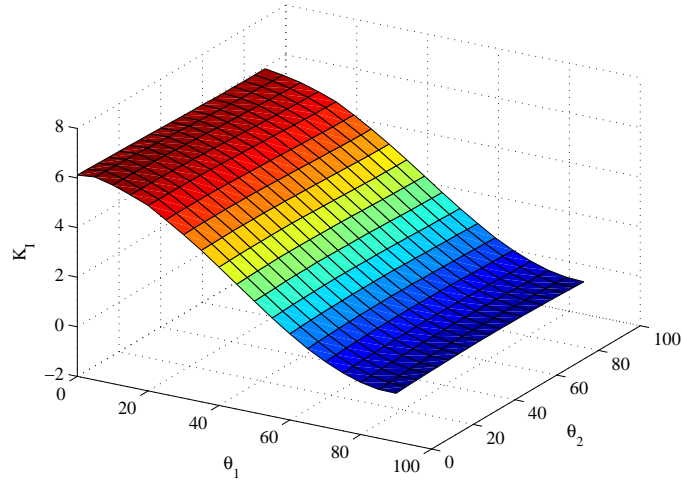
Figure 16: Influence of H/L ratio and $2a_2/2a_1$ on computed stress intensity factor.

(16) that as the ratio of crack lengths increases, the normalized mode I SIF also increases. And as the H/L ratio increases, all the curves approach the analytical solution ($K_{\text{analytical}}$). The values will not be equal to the analytical solution, because the analytical solution is computed for the case with one center crack.

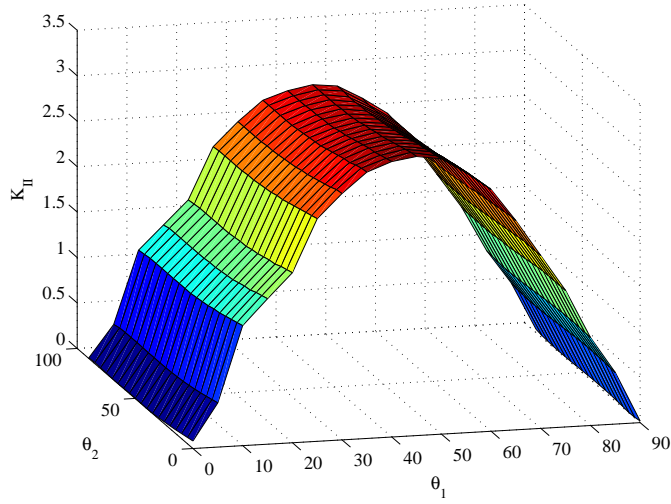
Next, the influence of the relative angle between the cracks on the mode I and the mode II SIF for a crack length of $2a_1 = 2a_2 = 0.2$, with the distance between the cracks: $H = 0.1$ and $L = 0.2$ is studied. Figure (17) shows the variation of mode I and mode II SIF with the angle subtended by the cracks to the horizontal axis. It is seen that with the increase in the angle of the crack, (θ_1 and θ_2), the mode I SIF decreases and approaches zero for $\theta_1 = \theta_2 = 90^\circ$. While the mode II SIF, initially increases with increase in the crack angle and reaches the maximum for the crack angle $\theta_1 = \theta_2 = 45^\circ$ and decreases with further increase in the angle.

4.5. Bimaterial bar

To illustrate the effectiveness of the proposed method to integrate weak discontinuities, we simulate a one-dimensional bimaterial bar discretized with 2D quadrilateral elements. Consider a two-dimensional square domain $\Omega =$



(a) mode I



(b) mode II

Figure 17: Plate with two cracks: the variation of mode I SIF and mode II SIF with respect to angle between the cracks for crack lengths $2a_1 = 0.2$ and $2a_2 = 0.2$. The distance between the cracks are: $H = 0.1$ and $L = 0.2$

$\Omega_1 \cup \Omega_2$ of length $L = 2$ with the material interface Γ located at $b = L/2$. The Young's modulus and Poisson's ratio in $\Omega_1 = (-1, b) \times (-1, 1)$ are $E_1 = 1$, $\nu = 0$, and that in $\Omega_2 = (b, 1) \times (-1, 1)$ are $E_2 = 10$, $\nu = 0$. With no body forces, the exact displacement solution with $u_y = 0$ at $y = -1$ and $u_y = 1$ at $y = 1$ is given by:

$$u(y) = \begin{cases} (y+1)\alpha, & -1 \leq y \leq b, \\ 1 + \frac{E_1}{E_2}(y-1)\alpha, & b \leq y \leq 1 \end{cases} \quad (14)$$

where,

$$\alpha = \frac{E_2}{E_2(b+1) - E_1(b-1)} \quad (15)$$

The relative error in displacement norm used to measure the accuracy of the results:

$$R.E_d = \sqrt{\frac{\sum_{i=1}^{\text{ndof}} (u_i^h - u_i^{\text{exact}})^2}{\sum_{i=1}^{\text{ndof}} (u_i^{\text{exact}})^2}} \times 100 \quad (16)$$

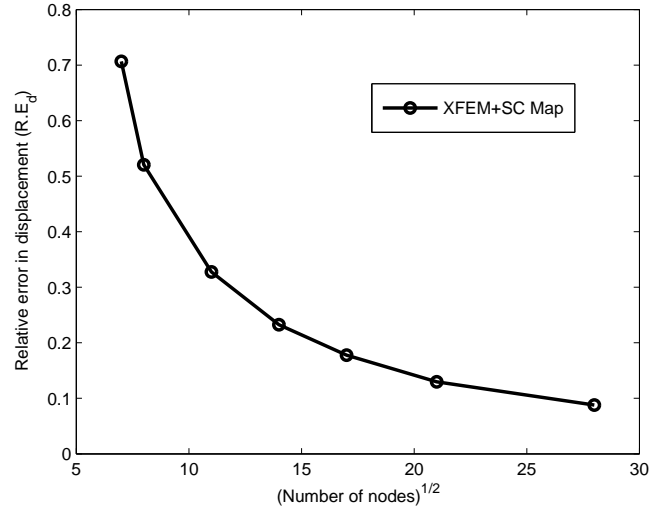
Figure (18) shows the relative error and the rate of convergence in the displacement norm. It is seen that with decrease in mesh density, the relative error in displacement norm also decreases. The rate of convergence is also shown in the Figure (18). The proposed method obtains convergence rate of 1.34 in the L_2 - norm, very close to the value reported in the literature [61]. The convergence rate is suboptimal due to the absence of treatment of the blending elements [59, 29, 56, 57].

Next, the influence of the material interface is studied. Three different configurations of the material interface are considered for the study (see Figure (19)).

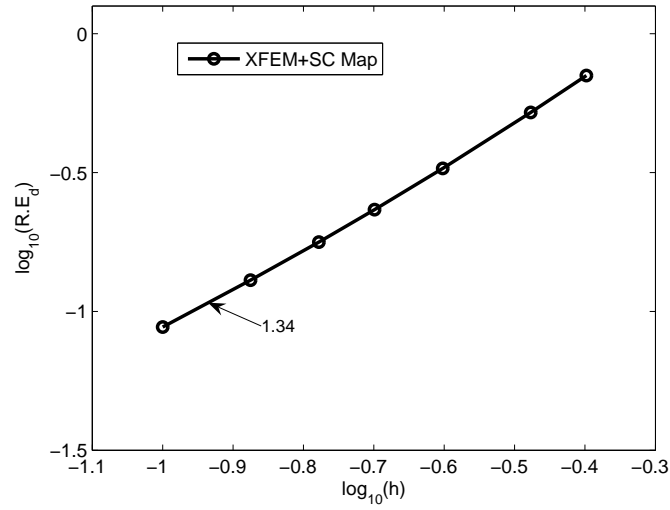
Figure (20) shows the strain energy convergence with mesh refinement for three different configurations. It is seen that the strain energy converges as the mesh is refined.

4.6. Double cantilever beam

The dimensions of the double cantilever beam (see Figure (21)) are 6×2 and the initial pre-crack with length of $a = 2.05$ is considered. The material properties are taken to be Young's modulus, $E = 100$ and Poisson's ratio,



(a)



(b)

Figure 18: Bimaterial problem: convergence in the displacement (L_2) norm: (a) the relative error and (b) the convergence rate. The method obtains convergence rate of 1.34 in the L_2 - norm

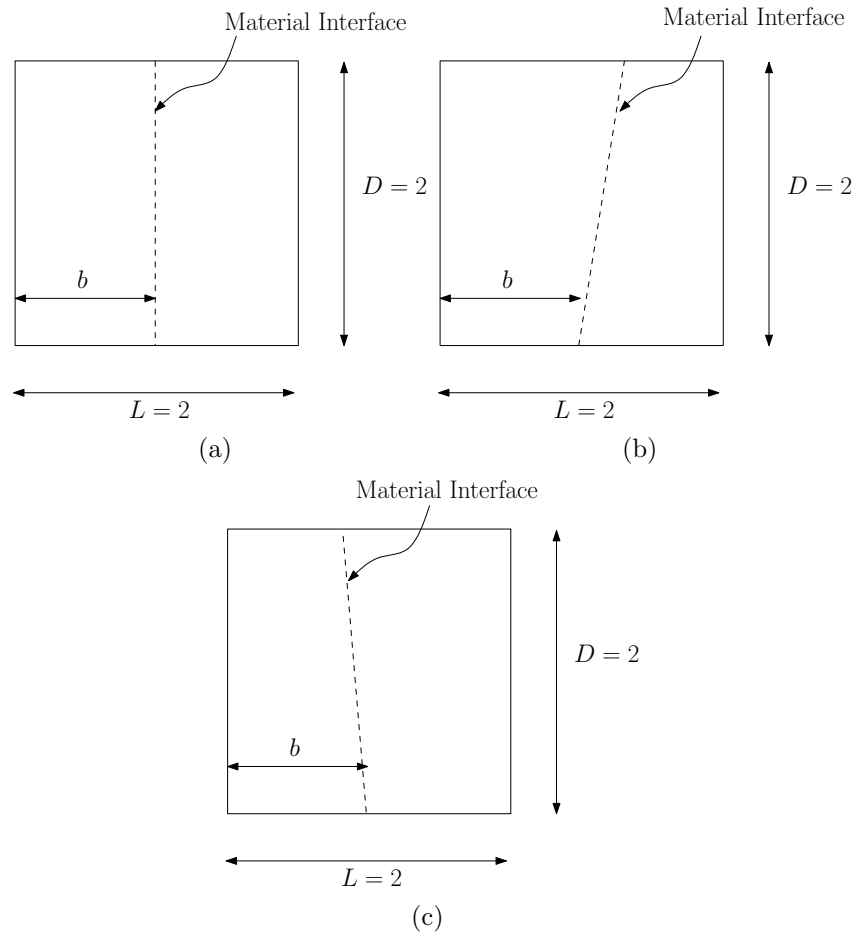


Figure 19: Bimaterial problem: (a) Straight Interface; (b) Slanted Interface (Positive slope) and (c) Slanted Interface (Negative slope)

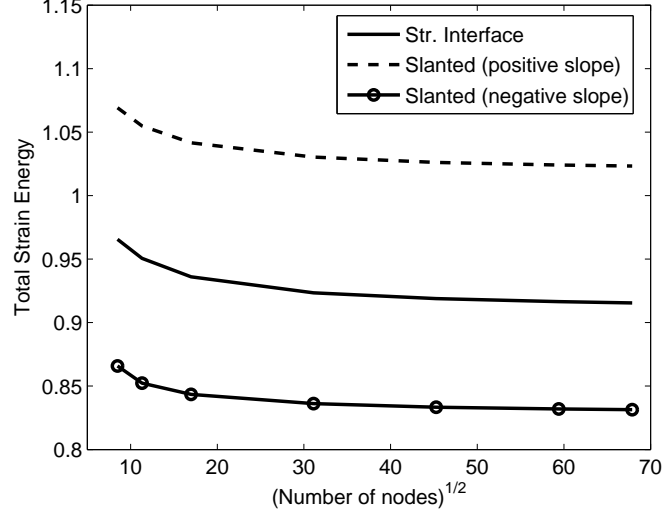


Figure 20: Bimaterial problem: convergence of the strain energy with mesh refinement

$\nu = 0.3$. And the load P is taken to be unity. By symmetry, a crack on the mid-plane of the beam is under pure mode I and the crack would propagate in a straight line, however, due to small perturbations in the crack geometry, the crack takes a curvilinear path [1]. A quasi-static crack growth is considered in this study and the growth is governed by the maximum hoop stress criterion [63], which states that the crack will propagate from its tip in the direction θ_c where the circumferential (hoop) stress $\sigma_{\theta\theta}$ is maximum. The critical angle is computed by solving the following equation:

$$K_I \sin(\theta_c) + K_{II}(3 \cos(\theta_c) - 1) = 0 \quad (17)$$

Solving Equation (17) gives the crack propagation angle [64]

$$\theta_c = 2 \arctan \left[\frac{-2 \left(\frac{K_{II}}{K_I} \right)}{1 + \sqrt{1 + 8 \left(\frac{K_{II}}{K_I} \right)^2}} \right] \quad (18)$$

The crack growth increment, Δa is taken to be 0.15 for this study and the crack growth is simulated for 8 steps. The domain is discretized with a structured mesh consisting of 1200 elements. The crack path is simulated

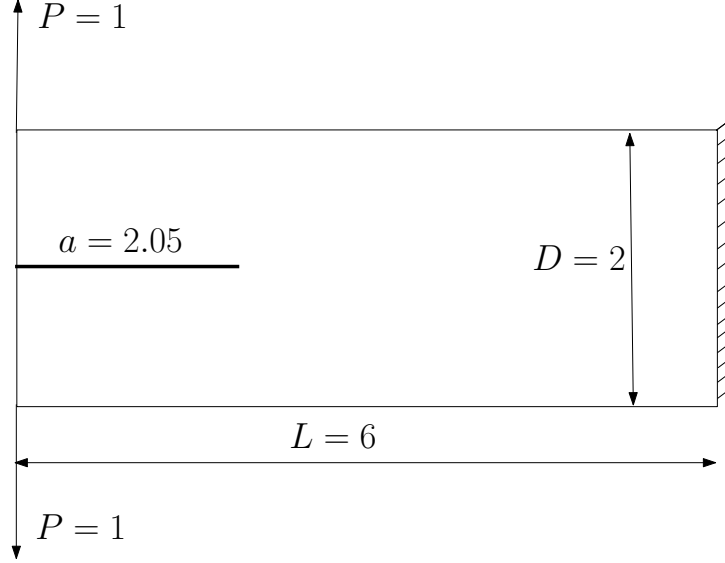


Figure 21: Geometry and loads of a double cantilever beam

using both methods and is shown in Figure (22). The crack path qualitatively agrees with the published results [1].

5. CONCLUSION

In this paper, we used the new numerical integration proposed for arbitrary polygons in [2] to integrate the discontinuous and singular integrands appearing in the XFEM stiffness matrix. The proposed method eliminates the need to sub-divide elements cut by strong or weak discontinuities or containing the crack tip. With a few examples from linear elastic fracture mechanics and a bimaterial problem, the effectiveness of the proposed method is illustrated. It is seen that for similar number of integration points, the proposed technique slightly outperforms the conventional integration method based on sub-division. With mesh refinement, both integration techniques provide convergence of the SIFs to the analytical SIFs. It seems possible that the proposed technique could serve as a way to integrate discontinuous approximations in the context of 3D problems as well, which will be the topic of forthcoming communications.

Acknowledgement The first author acknowledges the financial support of (1) the Overseas Research Students Awards Scheme; (2) the Faculty of

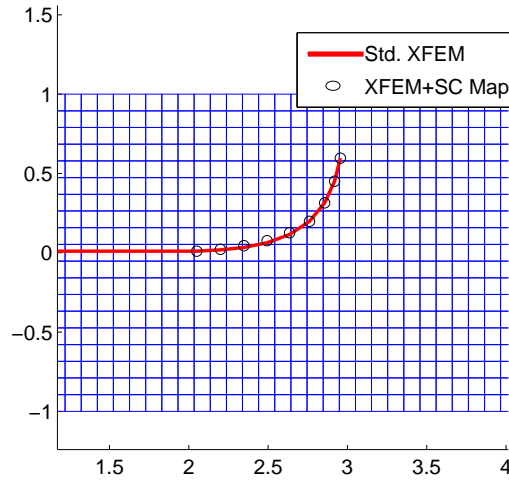
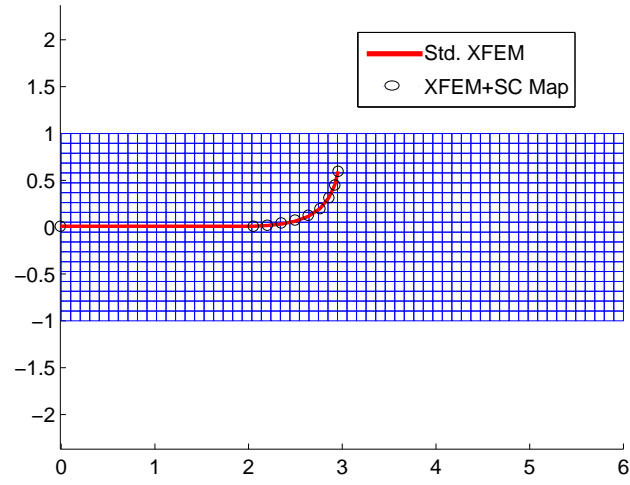


Figure 22: Double cantilever beam: comparison of crack path between the two numerical integration methods.

Engineering, for period Jan. 2009 - Sept. 2009 and of (3) the School of Engineering (Cardiff University) for the period Sept. 2009 onwards.

The last author gratefully acknowledge the financial support of the Royal Academy of Engineering and of the Leverhulme Trust for Senior Research Fellowship (2009-2010) [Towards the Next Generation Surgical Simulators] <http://www.raeng.ork.uk/research/researcher/leverhulme/current.htm>.

References

- [1] Belytschko T, Black T. Elastic crack growth in finite elements with minimal remeshing. *Int. J. Numer. Meth. Engng* 1999; **45**:601–620.
- [2] Natarajan S, Bordas SP, Mahapatra DR. Numerical integration over arbitrary polygonal domains based on schwarz-christoffel conformal mapping. *International Journal of Numerical Methods in Engineering* 2009; **80**(1):103–134, doi:10.1002/nme.2589.
- [3] Babuška I, Caloz G, Osborn J. Special finite element methods for a class of second order elliptic problems with rough coefficients. *SIAM Journal of Numerical Analysis* 1994; **31**:945–981.
- [4] Melenk JM. On generalized finite element methods. PhD Thesis, University of Maryland, College Park, MD 1995.
- [5] Möes N, Dolbow J, Belytschko T. A finite element method for crack growth without remeshing. *Int. J. Numer. Meth. Engng* 1999; **46**(1):131–150.
- [6] Strouboulis T, Babuška I, Copps K. The design and analysis of the generalized finite element method. *Computer Methods in Applied Mechanics and Engineering* 2000; **181**:43–96.
- [7] Simone A, Duarte C, der Giessendu EV. A generalized finite element method for polycrystals with discontinuous grain boundaries. *International Journal for Numerical Methods in Engineering* 2006; **67**:1122–1145.
- [8] Fries TP, Belytschko T. The intrinsic xfem: a method for arbitrary discontinuities without additional unknowns. *Int. J. Numer. Meth. Engng* 2006; **68**(13):1358–1385, doi:10.1002/nme.1761.

- [9] Duarte C, Babuška I, Oden J. Generalized finite element methods for three dimensional structural mechanics problems. *Computers and Structures* 2000; **77**:215–232.
- [10] Babuška I, Melenk J. The partition of unity finite element method. *International Journal for Numerical Methods in Engineering* 1997; **40**:727–758.
- [11] Babuška I, Banerjee U, Osborn J. Survey of meshless and generalized finite element methods: a unified approach. *Acta Numerica* 2003; **12**:1–125.
- [12] Hu N, Wang H, Yan B, Fukunaga H, Mahapatra DR, Gopalakrishnan S. The partition of unity finite element method for elastic wave propagation in reissner-mindlin plates. *International Journal for Numerical Methods in Engineering* 2007; **70**:1451–1479.
- [13] Chessa J. The extended finite element method for free surface and two phase flow problems. PhD Thesis, Northwestern University 2002.
- [14] Chessa J, Belytschko T. An enriched finite element method for axisymmetric two-phase flow with surface tension. *Journal of Computational Physics* 2003; .
- [15] Chopp D, Sukumar N. Fatigue crack propagation of multiple coplanar cracks with the coupled extended finite element/fast marching method. *International Journal of Engineering Science* 2003; **41**(8):845–869.
- [16] Duddu R, Bordas S, Moran B, Chopp D. A combined extended finite element and level set method for biofilm growth. *Int. J. Numer. Meth. Engng* 2008; **74**(5):848–870, doi:10.1002/nme.2200.
- [17] Ji H, Chopp D, Dolbow J. A hybrid extended finite element / level set method for modeling phase transformations. *International Journal for Numerical Methods in Engineering* 2002; **54**(8):1209–1233.
- [18] Merle R, Dolbow J. Solving thermal and phase change problems with the extended finite element method. *Computational Mechanics* 2002; **28**(5):339–350.

- [19] Wagner G, Moës N, Liu W, Belytschko T. The extended finite element method for Stokes flow past rigid cylinders. *International Journal for Numerical Methods in Engineering* 2001; **51**:393–413.
- [20] Liu X, Xiao Q, Karihaloo B. Xfem for direct evaluation of mixed mode sifs in homogeneous and bi-materials. *International Journal for Numerical Methods in Engineering* 2004; **59**(8):1103–1118, doi:10.1002/nme.906.
- [21] van der Bos F, Gravemeier V. Numerical simulation of premixed combustion using an enriched finite element method. *Journal of Computational Physics* 2009; **228**(10):3605–3624, doi:10.1016/j.jcp.2008.12.039.
- [22] Lecampion B. An extended finite element method for hydraulic fracture problems. *Communications in Numerical Methods in Engineering* 2009; **25**(2):121–133, doi:10.1002/cnm.1111.
- [23] Bordas S, Nguyen V, Dunant C, Nguyen-Dang H, Guidoum A. An extended finite element library. *Int. J. Numer. Meth. Engng* 2007; **71**(6):703–732, doi:10.1002/nme.1966.
- [24] Dunant C, Nguyen P, Belgasmia M, Bordas S, Guidoum A, Nguyen-Dang H. Architecture trade-offs of including a mesher in an object-oriented extended finite element code. *European journal of computational mechanics* 2007; **16**(16):237–258. Special issue on the extended finite element method.
- [25] Menk A, Bordas S. Influence of the microstructure on the stress state of solder joints during thermal cycling. *10th International Conference on Thermal, Mechanical and Multi-Physics Simulation and Experiments in Micro-Electronics and Micro-Systems*, Delft University of Technology, The Netherlands, 2009; 570–574.
- [26] Bordas A, Ronald H, Hoppe W, Petrova S. Mechanical failure in microstructural heterogeneous materials. *Lecture notes in computer science (LNCS) post-proceedings. Proceedings of the sixth international conference on numerical methods and applications* 2006; **6**:24–26.
- [27] Karihaloo B, Xiao Q. Modelling of stationary and growing cracks in fe framework without remeshing: a state-of-the-art review. *Computers and Structures* 2003; **81**(3):119–129, doi:10.1016/S0045-7949(02)00431-5.

- [28] Belytschko T, Gracie R, Ventura G. A review of extended/generalized finite element methods for material model. *Modelling and Simulation in Materials Science and Engineering* 2009; **17**(4):1–24.
- [29] Xiao B, Karihaloo B. Improving the accuracy of xfem crack tip fields using higher order quadrature and statically admissible stress recovery. *International Journal for Numerical Methods in Engineering* 2006; **66**(9):1378–1410.
- [30] Barros F, Proenca S, de Barcellos C. On the error estimator and p -adaptivity in the generalized finite element method. *Int. J. Numer. Meth. Engng.* 2004; **60**(14):2373–2398.
- [31] Strouboulis T, Zhang L, Babuska I. A posteriori error estimation for generalized finite element methods. *Computer Methods in Applied Mechanics and Engineering* 2006; **195**(9-12):852–879.
- [32] Belytschko T, Lu Y. Element-free galerkin methods for static and dynamic fracture. *International Journal of Solids and Structures* 1995; **32**:2547–2570.
- [33] Rabczuk T, Belytschko T, Xiao S. Stable particle methods based on lagrangian kernels. *Computer Methods in Applied Mechanics and Engineering* 2004; **193**:1035–1063.
- [34] Rabczuk T, Belytschko T. Adaptivity for structured meshfree particle methods in 2D and 3D. *International Journal for Numerical Methods in Engineering* 2005; **63**(11):1559–1582.
- [35] Bordas S, Duflot M. Derivative recovery and a posteriori error estimation in extended finite element methods. *Computer Methods in Applied Mechanics and Engineering* 2007; **196**(35-36):3381–3389, doi: 10.1016/j.cma.2007.03.011.
- [36] Bordas S, Duflot M, Le P. A simple a posteriori error estimator for the extended finite element method. *Communications in Numerical Methods in Engineering* 2008; **24**:961–971, doi:doi:10.1002/cnm.1001.
- [37] Rodenas J, Gonzalez-Estrada O, Tarancon J, Fuenmayor FJ. A recovery-type error estimator for the extended finite element method based on

- singular + smooth stress field splitting. *Int. J. Numer. Meth. Engng* 2008; **78**(4):545–571.
- [38] Ventura G. On the elimination of quadrature subcells for discontinuous functions in the extended finite-element method. *Int. J. Numer. Meth. Engng* 2006; **66**(5):767–795.
 - [39] Bordas SP, Rabczuk T, Hung NX, Nguyen VP, Natarajan S, Bog T, Quan DM, Hiep NV. Strain smoothing in FEM and XFEM. *Computers and Structures* 2009; doi:10.1016/j.compstruc.2008.07.006.
 - [40] Bordas SP, Natarajan S, Duflot M, Xuan-hung N, Rabczuk T. The smoothed finite element method. *8th World Congress on Computational Mechanics (WCCM8) and 5th European Congress on Computational Methods in Applied Sciences and Engineering (ECCOMAS 2008)*, 2008.
 - [41] Liu GR, Dai KY, Nguyen TT. A smoothed finite element for mechanics problems. *Computational Mechanics* May 2007; **39**(6):859–877, doi:10.1007/s00466-006-0075-4.
 - [42] Nguyen-Xuan H, Bordas S, Nguyen-Dang H. Smooth finite element methods: Convergence, accuracy and properties. *Int. J. Numer. Meth. Engng.* 2008; **74**(2):175–208, doi:10.1002/nme.2146.
 - [43] Chen JS, Wu CT, Yoon S, You Y. A stabilized conforming nodal integration for Galerkin mesh-free methods. *Int. J. Numer. Meth. Engng.* 2001; **50**:435–466.
 - [44] Natarajan S, Mahapatra DR, Bordas SP, Guo Z. A novel numerical integration technique over arbitrary polygonal surfaces. *Proceedings of the 17th UK National Conference on Computational Mechanics in Engineering, Nottingham, U.K.*, 2009.
 - [45] Natarajan S, Bordas SPA, Mahapatra DR. On numerical integration of discontinuous approximations in partition of unity finite elements. *Proceedings of IUTAM-MMS 2008, Indian Institute of Science, Bangalore, India.*, 2008.
 - [46] Balachandran G, Rajagopal A, Sivakumar S. Mesh free galerkin method based on natural neighbors and conformal mapping. *Computational Mechanics* 2008; **42**(6):885–905, doi:10.1007/s00466-008-0292-0.

- [47] Bordas S, Legay A. Enriched finite element short course: class notes. *The extended finite element method, a new approach to numerical analysis in mechanics: course notes*, Organized by S. Bordas and A. Legay through the EPFL school of continuing education, Lausanne, Switzerland, December 7–9, 2005 and July 2007.
- [48] Chen J, Wu C, Yoon S, You Y. A stabilized conforming nodal integration for galerkin meshfree-methods. *International Journal for Numerical Methods in Engineering* 2001; **50**:435–466.
- [49] Rabczuk T, Areias P, Belytschko T. A meshfree thin shell method for non-linear dynamic fracture. *International Journal for Numerical Methods in Engineering* 2007; **72**(5):524–548.
- [50] Rabczuk T, Belytschko T. A three dimensional large deformation mesh-free method for arbitrary evolving cracks. *Computer Methods in Applied Mechanics and Engineering* 2007; **196**(29-30):2777–2799.
- [51] Rabczuk T, Bordas S, Zi G. A three dimensional meshfree method for static and dynamic multiple crack nucleation/propagation with crack path continuity. *Computational Mechanics* 2007; **40**(3):473–495.
- [52] Bordas S, Rabczuk T, Zi G. Three-dimensional crack initiation, propagation, branching and junction in non-linear materials by an extended meshfree method without asymptotic enrichment. *Engineering Fracture Mechanics* 2008; **75**(5):943–960.
- [53] Suvrau D, Bathe K. The method of finite spheres with improved numerical integration. *Computers and Structures* 2001; **79**(22):2183–2196, doi:10.1016/S0045-7949(01)00124-9.
- [54] Peirce W. Numerical integration over the planar annulus. *Journal of the Society for Industrial and Applied Mathematics* 1957; **5**(2):66–73.
- [55] Driscoll A, Trefethen N. Algorithm 756: a matlab tool box for schwarz-christoffel mapping. *ACM Transactions on Mathematical Software* 1996; **22**:168–186.
- [56] Béchet E, Minnebo H, Moës N, Burgardt B. Improved implementation and robustness study of the X-FEM for stress analysis around cracks.

- Int. J. Numer. Meth. Engng.* 2005; **64**(8):1033–1056, doi:10.1002/nme.1386.
- [57] Laborde P, Pommier J, Renard Y, Salaün M. High-order extended finite element method for cracked domains. *International Journal for Numerical Methods in Engineering* September 2005; **64**(3):354–381, doi:10.1002/nme.1370.
 - [58] Chahine E, Laborde P, Renard Y. Crack tip enrichment in the xfem using a cutoff function. *International Journal for Numerical Methods in Engineering* August 2008; **75**(6):629–646, doi:10.1002/nme.2265.
 - [59] Chessa J, Wang H, Belytschko T. On the construction of blending elements for local partition of unity enriched finite elements. *International Journal of Numerical Methods in Engineering* 2003; **57**:1015–1038.
 - [60] Stazi FL, Budyn E, Chessa J, Belytschko T. An extended finite element method with higher-order elements for curved cracks. *Computational Mechanics* 2003; **31**:38–48.
 - [61] Fries TP. A corrected xfem approximation without problems in blending elements. *Int. J. Numer. Meth. Engng* 2008; **75**:503–532, doi:10.1002/nme.2259.
 - [62] Sih GC. Energy-density concept in fracture mechanics. *Engineering Fracture Mechanics* 1973; **5**:1037–1040.
 - [63] Erdogan F, Sih G. On the crack extension in plates under plane loading and transverse shear. *Journal of Basic Engineering* 1963; **85**:519–527.
 - [64] Sukumar N, Prévost JH. Modeling quasi-static crack growth with the extended finite element method part i: Computer implementation. *International Journal of Solids and Structures* 2003; **40**:7513–7537.

